# The aerodynamics development of the New Land Rover Discovery

**Conference Paper** · September 2017

# The aerodynamics development of the New Land Rover Discovery

Sébastien Chaligné, Ross Turner, Adrian Gaylard

Jaguar Land Rover

# Abstract

With ever stricter emissions regulations and the upcoming certification procedure defined in WLTP, the importance of aerodynamics for OEMs is increasing. This paper presents the aerodynamics development of the fifth generation Land Rover Discovery and gives an insight into the recent migration towards the use of new tools and processes to ensure future vehicles' compliance is achieved.

In the early development stages, numerical methods were exclusively used to optimise the main proportions of the vehicle, as well as to understand sensitivities and draw a road-map to attain the aerodynamics attribute targets. A full-scale test property ("Aerobuck") was then built and tested in the fixed-ground MIRA Full Scale Wind Tunnel (FSWT) to optimise specific areas in order to reduce the drag coefficient. These tests were done in combination with an extensive use of CFD to enable a better understanding of the flow fields and mechanisms involved. Finally, the development of an aerodynamically optimised wheel enabled the lowest drag coefficient to date for a Land Rover SUV, $C_D$=0.33.

Although certified in the MIRA FSWT, the validation process has also seen prototypes tested in the moving-ground FKFS Aeroacoustic Wind Tunnel (AAWT) benefiting from 5-belt ground simulation. A direct comparison between experimental and numerical results has also been made; they generally show good agreement between the two tools except for the prediction of so-called "cooling drag".

# 1 Introduction

With the introduction of new homologation regimes and stricter requirements for $CO_2$ emissions developing a new full-size SUV presents aerodynamic challenges. The New Discovery is Land Rover's fifth generation of this premium SUV. It replaces the Discovery 4, which was developed from the closely related Discovery 3, a vehicle that debuted in 2004.

The outgoing vehicle (Figure 1) illustrates the challenges. Designed to accommodate up to seven full-sized seats, with stadium seating and a command driving position, the exterior is characterised by largely vertical surfaces and a stepped roof line. The requirement for class-leading off road performance drove short front and rear overhangs. As a consequence the Discovery 3 was a bluff two-box SUV with a projected frontal area (A) of $3.15\text{m}^2$ and a drag coefficient ($C_D$) on launch of 0.41 [1], which reduced to less than 0.40 over subsequent model years. It was also developed using Jaguar Land Rover's previous generation of technical approaches: a test-lead

process focussed on fixed ground wind tunnel testing supported by a limited application of CFD [2, 3].

The development programme for the 2017 New Discovery aimed to maintain capability, such as off road performance and seating for seven adults, whilst delivering a new Design language compatible with future $CO_2$ requirements and the homologation philosophy embodied in WLTP. However, this left little scope for frontal area reduction and meant that aerodynamic improvement had to be approached via improved shape efficiency, i.e. reduced $C_D$.



Figure (1) - The Land Rover Discovery 3

The aerodynamic development of the New Discovery illustrates both the transition to new regulatory approaches and development processes, with CFD leading the development process [4] and wind tunnel testing transitioning to the use of a moving-ground facility.

## 2  Aerodynamic development process

The development process of the New Discovery consisted of four main stages: strategy, delivery, launch and production phases. The aerodynamic process is essentially embedded within the first three stages which will be described in the following section.

Throughout the development a number of tools have been used to assess the aerodynamics of the vehicle. In the strategy phase, the CFD software EXA PowerFLOW was exclusively used to optimise the main proportions of the vehicle, as well as to understand sensitivities and draw a road-map to attain the aerodynamics attribute targets. This is a commercially available CFD code, which provides a Very Large Eddy Simulation (VLES) turbulence model based on a Lattice Boltzmann (LB) solver [5, 6]. This inherently unsteady approach resolves the flow and any large scale unsteadiness on a regular cubic lattice with nested, hierarchical regions of enhanced

resolution. The effect of unresolved unsteady motions are accounted for by modifying the behaviour of the LB simulation, including an effective turbulent relaxation time, calculated via the RNG κ-ε transport equations [7]. It is a well-known development tool in the automotive industry and has been employed previously by Jaguar Land Rover in the aerodynamic development of vehicles such as the original Jaguar XF [8], Range Rover Evoque [3] and Jaguar XE [4]. The Discovery was also the first programme to benefit from a deployed soiling CFD simulation method [9]. Figure 2 shows that over half of the total number of CFD simulations was run in this early design phase.
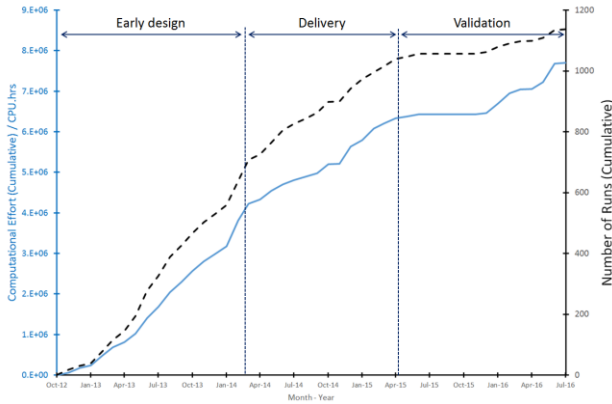


Figure (2) - Number of CPU hours used throughout the vehicle development

In the delivery phase, CFD was still used but in combination with experiments in the MIRA Full Scale Wind Tunnel (FSWT). This tunnel has a closed test-section open-return (NPL) lay-out with an informal return-path generated by its location in a large hanger. The test section floor is fixed, with no floor boundary layer control [10] and force measurements are made via an under floor balance, with the vehicle's non-rotating wheels sat on four pads reacting their load to the balance. The influence of blockage on force and pressure measurements is accounted for via a one-dimensional continuity correction [11]; an additional correction is made to the measured drag coefficient accounting for the longitudinal pressure gradient.

Validation prototype vehicles became available in the launch phase enabling the aerodynamic performance to be signed off against the target. Testing of these prototypes was undertaken primarily in the FSWT for consistency with development targets; however, some exploratory testing was also conducted in the AAWT to aid

understanding in preparation for the upcoming changes in certification procedures. The Aeroacoustic Wind Tunnel of Stuttgart University has been extensively developed for automotive aerodynamic purposes over several decades [12]. The test vehicle is set on a 5-belt system with restraint struts holding it in position [13]. This set up enables a better representation of the on-road conditions compared to the FSWT by simulating the relative motion between the vehicle and road, as well as wheel rotation.

## 2.1 Early Design Characterisation

The early design phase consisted of two main parallel work-streams, both completed exclusively numerically. First the volume and proportions of the vehicle were optimised to ensure compatibility between the Design vehicle vision and aerodynamic attribute targets, whilst identifying the drag sensitive areas around the vehicle and develop a road-map designed to deliver the aerodynamic drag target.

Second, characterisation work enabled drag reduction opportunities to be identified and quantified. These ideas were progressed with the Engineering and Design teams to develop and refine the roadmap to target, as per the example shown in Figure 3.
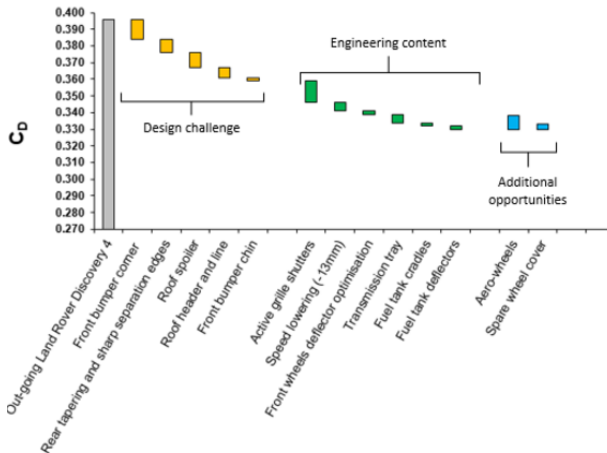


Figure (3) - Example of early design road-map to deliver the aerodynamic attribute drag target

It was clear from the start that to deliver the requisite step-change in drag a significant departure from the exterior Design of the out-going Discovery would be required.

Collaboration with Design started very early in the programme, enabling the team to influence the initial exterior themes. For example, work was done to minimise the drag impact of the stepped roof – enabling the preservation of a signature Discovery feature that improves interior roominess. Other important areas of development were the front corners, rear fenders and tailgate spoiler.

## 2.2 Delivery Phase

Once a single Design Theme was chosen and the engineering content finalised, detailed optimisation began. CFD was used to understand geometric sensitivities and guide development. The full-size "aerobuck" test property, shown in Figure 4, was built to facilitate detailed optimisation through collaboration with Designers, enable surface contamination testing and increase confidence in numerical vehicle drag predictions. This was constructed using a milled foam top-hat on a donor Range Rover underfloor. Inter-changeable modules for key areas, such as Air Curtain and Spoiler enabled efficient use of tunnel time.



Figure (4) – Photographs of the New Discovery "aerobuck" being tested at MIRA

A number of tests were conducted jointly with the Designer and Clay Modellers to optimise details such as the Rear Lamps and Spoiler Winglets. The following section details some of the features developed during this delivery phase.

### 2.2.1 Air Curtains

In the early design stage, the front corners were clearly identified as one the most promising areas for drag reduction with an overall potential of about 15 counts (1 count = 0.001 $C_D$). Improvement was realised through a combination of conventional

shape optimisation and the development of an Air Curtain. The geometry was optimised as far as possible whilst staying true to the Design vision – a combination of increasing front wheel coverage, having a more vertical wheel arch ribbon and increasing the convexity of the profile in plan-view to get more suction locally. An Air Curtain was then introduced to further control the flow.
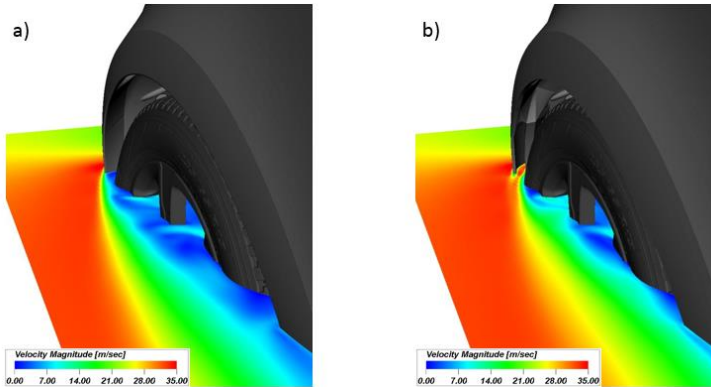


Figure (5) – Effect of air curtain on the flow field (Horizontal slice +150mm from wheel centre): a) without and b) with air curtain

A comprehensive CFD study was conducted to characterise drag sensitivity to the key geometric parameters of the Air Curtain and understand subsequent changes to the flow. From this three concepts were developed and tested on the "Aerobuck" in both moving and static ground wind tunnels showing potential to reduce drag by up to 6 counts.

As seen in Figure 5, the Air Curtain compensates for some of the lack of longitudinal flow momentum near the body side due to a large angle of flow separation at the front wheel arch liner, laterally kicking the flow away from the side panels.

## 2.2.2 Under-floor

A key challenge for the New Discovery was developing an aerodynamic under-floor with best in class off-road capability and robustness. An aerodynamically efficient floor is usually achieved by maintaining as much longitudinal flow momentum as possible as well as managing flow separations. The aerodynamic floor strategy is presented in Figure 6.
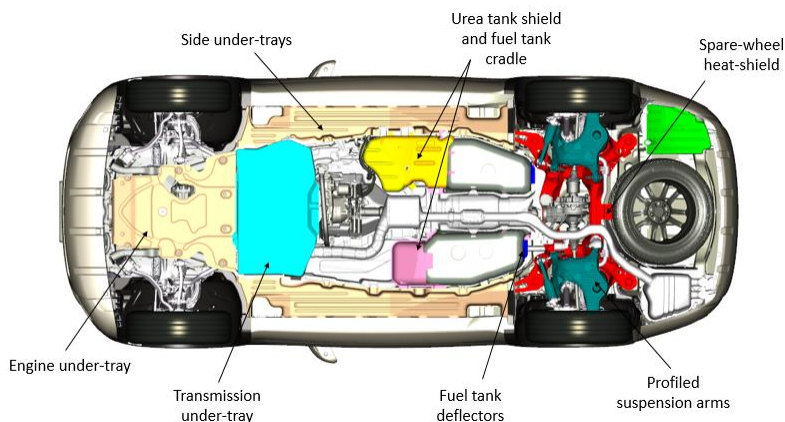
Figure (6) – Aerodynamic under-floor strategy

The engine and side under-trays were carried over from previous vehicles sharing this architecture. The large aluminium transmission under-tray has been clad in a smooth skin giving an incremental 3 drag count benefit and improving NVH performance. Its trailing edge has been tuned to slightly deflect the flow down to create a stable recirculation bubble at the break-over x-location, thus maintaining flow momentum. The flow re-attaches onto the exhaust SCR can at the vehicle centreline and onto the urea and fuel tank cradles as illustrated in Figure 7 a). These protective shields have been extended to maximise coverage and profiled to ensure minimal stagnation pressure.
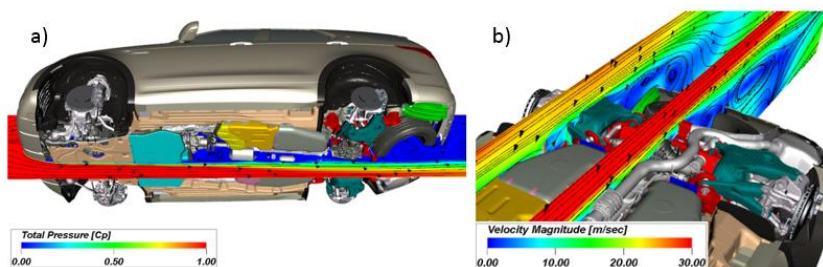


Figure (7) – CFD results illustrating the final flow field under the production vehicle: a) total pressure coefficient vertical slice at vehicle centreline and b) velocity magnitude vertical slices at centreline and offset by 0.5m

The large radius used on the lower trailing edge of the fuel tank cradle to avoid grounding was initially adverse for drag, causing the flow to turn upwards in an unsteady manner. Deflectors have been developed to guide the flow more efficiently and preventing it from impinging on the sub-frame and suspension arms. This resulted in a drag reduction of 2 counts.

The heat shield surrounding the spare wheel was optimised to give the required thermal protection without a drag penalty. For powertrains with a single sided exhaust muffler, an in-fill tray was engineered to bridge the void between the suspension and rear bumper.

Eventually, the development of a low-drag wake was achieved by forcing the flow to separate steadily over time along the y-axis, at the same x-location. At the vehicle centreline, the heat-shield z-location was optimised to ensure separation at this location, thus enabling the drag to be insensitive to the presence of the underslung spare wheel, or its size. Outboard of the centreline, the rear suspension arm trailing edge was used to force separation as illustrated in Figure 7 b).

### 2.2.3 Slotted roof spoiler

Rear surface contamination is essentially an aerodynamically driven issue [14] and was identified as an area for improvement over the out-going model. To address this, a roof spoiler with slots creating a secondary flow tangent to the rear glass was developed. Previous studies on square back cars [15, 16] and trucks [17] have shown that a large reduction of rear glass soiling can be achieved using this technique, but usually at the expense of a significant drag coefficient increase.

Many different spoiler configurations were tested for both aerodynamics and soiling in the FKFS Aeroacoustic and Thermal wind tunnels respectively and in CFD. The greater the flow rate through the slots, the greater the reduction in rear soiling, but at high flow rates this results in a significant detriment to the drag coefficient as well as a large increase in rear lift. Configurations of slot were identified with a moderate flow rate which nevertheless enables an improvement of 15 to 30% in rear glass cleanliness and are neutral for drag, or even offer a small benefit.

Figure 8 shows the wake structure at the vehicle centreline as well as the static pressure coefficient ($C_p$) distribution over the base. Although the overall wake structure does not change significantly, the introduction of a span-wise vortex structure behind the rear glass can be seen. Even though the presence of this structure reduces the static pressure on the glass and increases the drag locally as seen in Figure 9, the pressure recovery in the tailgate area is greater which cancels out the negative impact on the base drag.
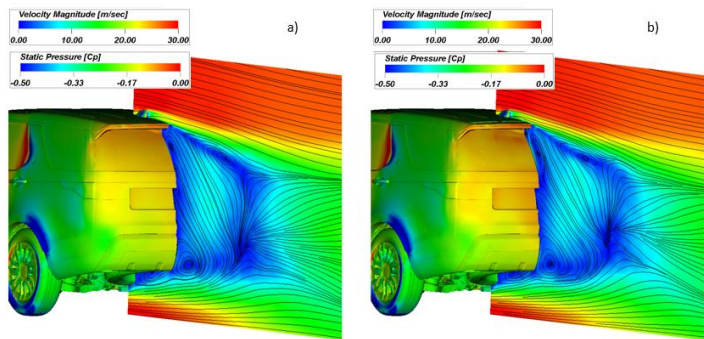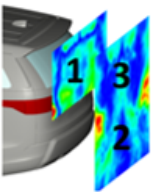
Figure (8) – Effect of the slotted spoiler on base pressure and velocity magnitude at vehicle centreline: a) without and b) with slotted spoiler

Figure 9 highlights the subtle wake re-organisation causing the increase in pressure recovery over the tailgate. The span-wise vortex structure draws down the top shear layer slightly, reducing the height of the recirculation areas as well as providing a better condition for the side shear layers above and below the vehicle waistline, resulting in a less squeezed wake at mid-height. The local drag $C_{Dl}$ (originally termed "micro-drag"), defined in Cogotti [18] and provided in Table 1 illustrates the increase in drag behind the rear glass with the slotted spoiler but also the resulting overall improvement downstream. This specific configuration resulted in a drag reduction of 3 counts. The rear glass soiling benefit seen during on-road testing was measured to be about 20%.

In addition to the spoiler, the winglets shown in Figure 8 bring an additional benefit of 2 drag counts compared to the configuration without them, illustrated in Figure 9.

Table (1) – Local drag coefficient in the vehicle near wake for vehicle with and without slots

| | | Without slots | | | Slotted spoiler | | |
|---|---|---|---|---|---|---|---|
| | | $C_{Dl}$ | $C_{Dv}$ | $C_{Dw}$ | $C_{Dl}$ | $C_{Dv}$ | $C_{Dw}$ |
|  | Slice 1 | **0.077** | 0.005 | 0.072 | **0.082** | 0.005 | 0.077 |
| | Slice 2 | **0.095** | 0.006 | 0.089 | **0.090** | 0.006 | 0.084 |
| | Slice 3 | **0.105** | 0.005 | 0.100 | **0.103** | 0.004 | 0.099 |
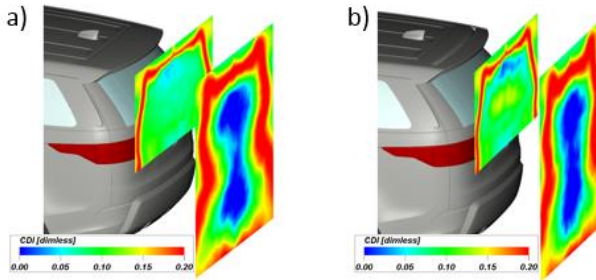
Figure (9) – Effect of the slotted spoiler on local drag coefficient: a) without and b) with slotted spoiler

### 2.2.4   Eco-wheel

A $CO_2$ focused wheel and tyre combination was engineered for this programme, consisting of a narrow 235 mm (nominal) width, low rolling resistance tyre with an aerodynamically optimised 20" wheel style. Two design themes were developed for the wheel using guidelines supplied by the Aerodynamics Team. A sensitivity study was conducted to guide the optimisation of the preferred theme. A summary of the configurations tested is shown in Table 2 along with their respective numerically predicted changes in drag coefficient $C_D$, the fan or ventilation moment $C_{D,VENT}$ [19 - 22] given in equivalent $C_D$ and the brake cooling coefficient BCC. A scaled version of the 21" wheel offered on Range Rover hybrids was used as a baseline – representing a well performing wheel.

Table (2) – Influence of geometrical wheel changes on $C_D$, fan moment $C_{D,FM}$ and BCC

|  | BASELINE | 1 | 2 | 3 | 4 | 5 | 6 / FINAL |
|---|---|---|---|---|---|---|---|
| WHEEL STYLE | Range Rover HEV wheel | Cyclone as received | As 1 with chamfers on spokes | As 1 with thinner spokes | As 1 without back star | Concave annular blanking | Convex annular blanking |
|  |  |  |  |  |  |  |  |
| $\Delta C_D$ | - | -0.006 | -0.007 | -0.006 | -0.008 | -0.005 | -0.008 |
| $\Delta C_{D,VENT}$ | - | +0.001 | +0.001 | +0.001 | +0.001 | +0.001 | +0.001 |
| $\Delta$BCC | - | -1BCC | -1BCC | 0 | 0 | -1BCC | -1BCC |

Configuration 1 results in a drag benefit of 6 counts and shows a good Design interpretation of the aerodynamics guidelines, whilst not significantly degrading brake cooling. Configurations 2 and 3 show attempts to change the wheel fan moment which eventually remained within a (effective) drag count during the study.
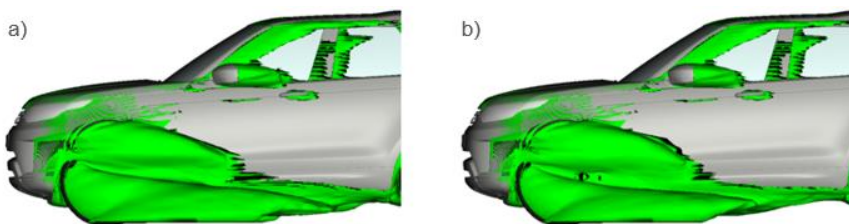


Figure (10) – Iso-surface of total pressure coefficient $CpT = 0$ for configuration: a) 5 and b) 6

The sensitivity study also identified annular blanking of the radial profile as the critical parameter for this wheel design, consistent with the findings of other workers [23]. Going from a concave profile to a convex profile laterally more flush to the outermost face of the rim induces more positive longitudinal entrainment of the flow near the ground, thus reducing the length of the lower structure originating from the flow separation around the tyre shoulder. This change of wheel wake structure observed in Figure 10 unlocks an additional 3 drag counts with minimal impact on Design and feasibility.

Eventually style 6 with a black and diamond turn finish was chosen as the wheel style moving forward. This wheel presented in Figure 11 reduces the drag by 8 counts.



Figure (11) – Aerodynamic "Eco-wheel" developed for the 17MY Discovery

### 2.2.5 Active devices

To aid delivery of the aerodynamic target and help balance the other attributes of the vehicle, active devices have also been employed. The vehicle is offered with air suspension, which provides enhanced off-road capability and allows the car to automatically lower the ride height when cruising at motorway speeds. This reduces drag by 6 counts (uncorrected for frontal area change) at speeds where aerodynamic drag represents a significant proportion of the road load.

Active grille shutters are fitted to the upper cooling aperture allowing cooling airflow to be optimised to the driving conditions.

## 2.3 Validation and correlation

Testing of validation prototype vehicles was done predominately in the FSWT for consistency with development, however some exploratory testing was also conducted in the AAWT to aid understanding in preparation for the upcoming changes in certification procedures. This confirmed that a drag coefficient of $C_D = 0.33$ had been achieved in both wind tunnels – the lowest to-date for a Land Rover and a 17% improvement over the outgoing model.



Figure (12) – New Land Rover Discovery VP at FKFS wind tunnel (left) and CFD model as per FKFS configuration (right)

Although previous experience with the FSWT has shown good correlation between numerical and experimental results for SUVs, usually within ±5 counts for the predicted drag coefficient, the increased complexity due to modelling rotating wheels as well as the flow structures associated with the tyre tread and contact patch highlighted the need to correlate the tools with the new methods.

A correlation exercise was carried out on a validation prototype vehicle equipped with a 2.0 I4 Diesel engine and the 20'' Aerodynamic wheel discussed previously fitted with 235/60 Continental Cross Contact tyres. The CFD runs were specified with a low-blockage (0.1%) domain and a moving ground plane. Rotating velocity boundary conditions were applied to de-featured axisymmetric tyres whilst the rim and spokes were rotated using a sliding mesh (LRF) zone. Unfortunately, this setup does not capture the geometrical contact patch and the loaded tyre deformation as the tyre intersects with the ground. Also, a slight difference of 5mm in ride heights between the CFD model and the vehicle tested in the tunnel was corrected for by adding 2 counts to the physically measured value.

The absolute drag coefficients for this vehicle in two different cooling configurations are given in Table 3. Blanking all the front apertures results in a drag reduction of 15 counts in the wind tunnel; however, the drag delta predicted in CFD is about 1 count only. Predicting the cooling drag delta is known to be a difficult task [24] as it involves many flow field interactions around the vehicle [25] and this lack of correlation was expected.

Table (3) – Cooling drag deltas of the prototype measured in the AAWT and predicted in CFD

| Vehicle configuration | AAWT | CFD |
|---|---|---|
| Cooling drag delta | 0.015 | 0.001 |



Figure (13) – Wind tunnel corrections for the vehicle prototype with all cooling apertures open

Using the 2-gradient method for open jet wind tunnels of Mercker and Cooper [26, 27], a correction of + 12 drag counts was applied to the measured drag to account for the pressure gradient and the blockage in the test section. Moreover, the additional aerodynamic drag of the restraining struts increases the overall measured value by 2 counts [28], bringing the total wind tunnel correction to + 10 counts. Figure 13 illustrates the different corrections applied to the raw experimental data and highlights an excellent agreement - within 2 drag counts between the absolute drag values predicted by the two tools when the cooling apertures are open.

Obviously, the closed cooling configuration does not correlate as well. A comparison of some of the drag coefficient deltas induced by a number of configuration changes is given in Figure 14. Overall, the trends when modifying the under-floor are well captured by CFD although the drag delta magnitudes are not in perfect agreement. Removing the spare wheel resulted in a benefit of 1 drag count measured in the wind tunnel and almost 2 counts in CFD. This is an interesting result as previous tests in the FSWT and in CFD using a static ground boundary condition had shown no sensitivity in this area. This difference is believed to be due to the increase of momentum under the vehicle in moving ground configuration which makes the flow partially reattach onto the spare-wheel. This is illustrated in Figure 15, which shows the difference in static pressure predicted by CFD at the centreline between static and moving ground configurations for the same vehicle geometry. This mechanism also lowers the pressure behind the rear bumper, leading to the small drag detriment.

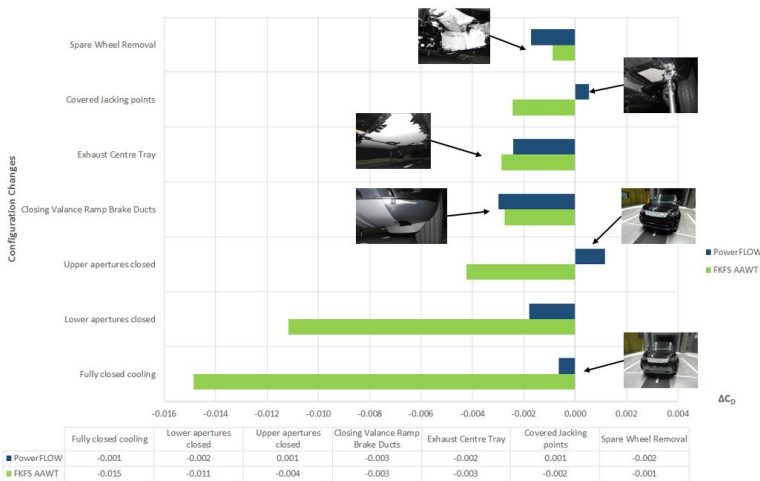| | Fully closed cooling | Lower apertures closed | Upper apertures closed | Closing Valance Ramp Brake Ducts | Exhaust Centre Tray | Covered Jacking points | Spare Wheel Removal |
|---|---|---|---|---|---|---|---|
| PowerFLOW | -0.001 | -0.002 | 0.001 | -0.003 | -0.002 | 0.001 | -0.002 |
| FKFS AAWT | -0.015 | -0.011 | -0.004 | -0.003 | -0.003 | -0.002 | -0.001 |

Figure (14) – Comparison of the experimental and numerical drag coefficient deltas induced by configuration changes

The trend is predicted incorrectly when covering the jacking points, as CFD predicts a small drag detriment whereas a 2 count benefit is measured in the wind tunnel. The reason for this discrepancy is not fully understood but plausible explanations may be the presence of the restraining struts in the tunnel which may be affecting the flow over the jacking points, or the tyre modelling simplifications that might result in wheel wake differences. Blanking the brake cooling valance ramps resulted in a drag reduction of 3 counts with both tools.
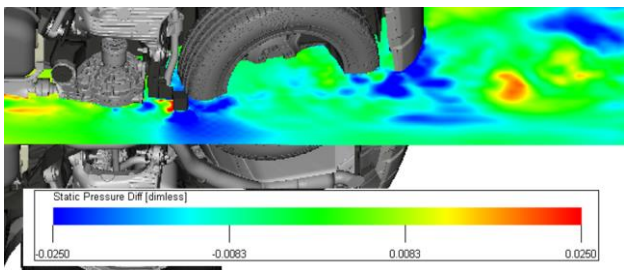


Figure (15) – CFD prediction of the static pressure coefficient difference between static and moving ground boundary conditions for the same vehicle geometry

Some alternative cooling configurations have also been compared by blanking the upper or lower cooling apertures. As for the fully closed cooling configuration, the different drag benefits measured in the wind tunnel are not agreement with the CFD predictions. The predicted trend is even incorrect: when blanking the upper aperture CFD predicts an increase in drag. These results again highlight the difficulties in predicting cooling drag and the importance of investigating this problem to get a better understanding on it.

This correlation exercise in moving ground rotating wheel conditions for a large SUV was the first of its kind within Jaguar Land Rover and shows a good agreement between our new CFD approach and the experiments in the AAWT. It also validates the aerodynamic development process for future vehicles which involve an exclusive usage of CFD in the early design phase, until a physical property is available.

# 3   Summary

Some elements of the aerodynamic development process of the New Land Rover Discovery have been described. To deliver the ambitious aerodynamic drag target, the out-going model underwent a spectacular transformation, enabling the drag coefficient to be reduced by 70 counts, down to $C_D$=0.33, the lowest figure to date for a Land Rover SUV.

To enable such a drag reduction, an optimisation of the main vehicle proportions, combined with some new elements of the under-body and an aerodynamic wheel were needed. A number of features reducing the overall drag further have also been presented.



Figure (16) – CFD rendering of the J#1 CFD model of the new Land Rover Discovery

Throughout its development, the Land Rover Discovery has seen some important changes in processes and best practices to prepare for the future certification procedures, moving from the static ground wind tunnel of MIRA to the moving-

ground FKFS wind tunnel and using new CFD boundary conditions with moving ground rotating wheels.

A correlation study has shown a good agreement between CFD and FKFS drag measurements, once wind tunnel corrections are applied. Apart from the cooling drag prediction, the trends when making configuration changes were also identical with similar magnitudes.

# Bibliography

1. Howell, J., Gaylard, A., Improving SUV Aerodynamics, 6th MIRA International Vehicle Aerodynamics Conference, p.1-17, 2006.

2. Gaylard, A.P., The Appropriate Use of CFD in the Automotive Design Process. SAE Technical Paper 2009-01-1162, 2009.

3. Samples, M., Gaylard, A. P., Windsor, S., The Aerodynamics Development of the Range Rover Evoque, 8th MIRA International Conference on Vehicle Aerodynamics, 2010.

4. Gaylard, A., The new Jaguar XE: a case study in computational aerodynamics, International Forum Advanced Automotive Aerodynamics, 2015.

5. Chen, H., Chen, S., and Matthaeus, W. H., Recovery of the Navier-Stokes equations using a lattice-gas Boltzmann method. Phys. Rev. A, **45**(8):R5339-R5342, 1992.

6. Chen, H., Teixeira, C., and Molvig, K., Digital physics approach to computational fluid dynamics: some basic theoretical features, Int. J. Mod. Phys. C, 8(4):675-684, 1997.

7. Chen, H., Kandasamy, S., Orszag, S., Shock, R., et al., Extended Boltzmann kinetic equation for turbulent flows. Science, 301(5633): 633-636, 2003.

8. Gaylard A.P., The Aerodynamic Development of the New Jaguar XF, 7th MIRA International Conference on Vehicle Aerodynamics, 2008.

9. Gaylard, A., Pitman, J., Jilesen, J., Gagliardi, A. et al. (2014). Insights into Rear Surface Contamination Using Simulation of Road Spray and Aerodynamics. SAE Int. J. Passeng. Cars - Mech. Syst., 7(2):673-681

10.Newnham, P., Passmore, M., Howell, J., Baxendale, A., On the Optimisation of Road Vehicle Leading Edge Radius in Varying Levels of Freestream Turbulence, SAE Technical Paper 2006-01-1029, 2006.

11. Carr, G. and Stapleford, W., Blockage Effects in Automotive Wind-Tunnel Testing, SAE Technical Paper 860093, 1986.

12. Künstner, R., Potthoff, J., Essers, U., The Aero-Acoustic Wind Tunnel of Stuttgart University, SAE Technical Paper 950625, 1995.

13. Blumrich, R., Widdecke, N., Wiedemann, J., Michelbach, A. et al., New FKFS Technology at the Full-Scale Aeroacoustic Wind Tunnel of University of Stuttgart, SAE Int. J. Passeng. Cars - Mech. Syst. 8(1):294-305, 2015.

14. Gaylard, A.P., Kirwan, K., Lockerby, D.A., Surface contamination of cars: a review, Proceedings of the Institution of Mechanical Engineers, Part D: Journal of Automobile Engineering, 2017

15. Janson, J., Darrieutort, L., Bannister, M., New development and working methods used in the aerodynamic development of the new large estate, JSAE paper 20005352, 2000.

16. Costelli, A.F., Aerodynamic characteristics of the Fiat UNO car, SAE paper 840297, 1984.

17. Fujimoto, T., Miyake, N., Watanabe, Y., Suppression of mud adhesion to the rear surface of a van-type truck, SAE paper 920203, 1992.

18. Cogotti, A., A Strategy for Optimum Surveys of Passenger-Car Flow Fields, SAE Technical Paper 890374, 1989.

19. Wickern, G., Zwicker, K., and Pfadenhauer, M., Rotating Wheels - Their Impact on Wind Tunnel Test Techniques and on Vehicle Drag Results, SAE Technical Paper 970133, 1997.

20. Landström C., Josefsson L., Walker T. and Löfdahl L., An experimental investigation of wheel design parameters with respect to aerodynamic drag, 8th FKFS Conference, 2011

21. Modlinger F., Demuth R. and Adams N., New Directions in the Optimization of the Flow around Wheels and Wheel Arches, MIRA International Conference on Vehicle Aerodynamics, 2008.

22. Vdovin, A., Lofdahl, L., and Sebben, S., Investigation of Wheel Aerodynamic Resistance of Passenger Cars, SAE Int. J. Passeng. Cars - Mech. Syst. 7(2):639-645, 2014.

23. Landström, C., Walker, T., Christoffersen, L., and Löfdahl, L., Influences of Different Front and Rear Wheel Designs on Aerodynamic Drag of a Sedan Type Passenger Car, SAE Technical Paper 2011-01-0165, 2011.

24. Larson, L., Gin, R., and Lietz, R., Aerodynamic Investigation of Cooling Drag of a Production Sedan Part 2: CFD Results, SAE Int. J. Passeng. Cars - Mech. Syst. 10(1):2017.

25. Pitman, J., An experimental investigation into the flow mechanism around an SUV in open and closed cooling air conditions, FKFS – 11th Aerodynamic Conference, 2017.

26. Mercker, E., Cooper, K., A Two-Measurement Correction for the Effect of a Pressure Gradient on Automotive, Open-Jet, Wind Tunnel Measurements. SAE Paper 2006-01.0568, 2006.

27. Mercker, E., On Buoyancy and Wake Distortion in Test Sections of Automotive Wind Tunnels, FKFS – 9th Aerodynamic Conference, p. 205-227, 2013.

28. Wiedemann, J., Potthoff, J., The New 5-Belt Road Simulation System of the IVK Wind Tunnels - Design and First Results SAE Technical Paper 2003-01-0429, 2003.

## Acknowledgements